Articles

From Chemical to Structural Order of Electrodeposited Ni22P Alloy: An XPS and EDXD Study

B. Elsener,[†] D. Atzei,[†] A. Krolikowski,[‡] V. Rossi Albertini,[§] C. Sadun,[||] R. Caminiti,[||] and A. Rossi[†,*]

Dipartimento di Chimica Inorganica e Analitica, Università degli Studi di Cagliari, Unità INSTM, Campus di Monserrato, I-09100 Italy, Institute of Solid State Technology, Department of Chemistry, Warsaw University of Technology, PL 00-664 Warsaw, Poland, Istituto di Struttura della Materia CNR, Area di Ricerca di Tor Vergata, Via del Fosso del Cavaliere 100, 00133 Roma, Italy, and Dipartimento di Chimica, Istituto Nazionale di Fisica della Materia, Università "La Sapienza" di Roma 1, P.le Aldo Moro 5, 00185 Roma, Italy

Received August 28, 2003. Revised Manuscript Received May 15, 2004

Amorphous electrodeposited nickel−phosphorus alloys with 22 at. % of phosphorus (Ni22P) have been analyzed in the amorphous and re-crystallized state by EDXD and XPS surface analysis. The re-crystallization kinetics have been determined following in situ structural changes by EDXD. Distinct diffraction patterns indicating the presence of Ni_3P confirm alloy re-crystallization at 645 °C. The XPS results show that all the core level binding energies of nickel such as $Ni2p_{3/2}$ and $Ni2p_{1/2}$ and phosphorus (P2p, P2s) remained constant after the change from X-ray amorphous to crystalline structure of the NiP alloy. Differences observed were as follows: (a) the binding energy difference between the Ni2p main lines and the satellite, (b) the fine structure of the NiLMM Auger lines, and (c) the density of states in the valence band in the region of the Ni3d electrons. On the basis of these results from EDXD and XPS, it can be concluded that the change in alloy structure from X-ray amorphous to crystalline influences the electronic structure of the NiP alloy but not the chemical state of phosphorus. An explanation based on the screening model proposed in the literature is discussed.

Introduction

Electroless deposited Ni−P alloys have many industrial applications[1] owing to their bright appearance, good mechanical properties, high hardness, and outstanding corrosion[2,3] and wear resistance as well as catalytic properties.[4] For these reasons, wide applications were found in the electronic industry as an underlayer in thin film memory disks.[5,6] These excellent technological properties, however, are closely related to the amorphous structure of the electrodeposited Ni−P alloys. It is well-established that electroless deposited alloys with phosphorus content P < 7 wt % are crystalline whereas at P > 9 wt % the alloys have an X-ray amorphous structure.[7,8] High phosphorus contents to reach the eutectic (ca. 11.5 wt %, 20 at. %) or hypereutectic compositions can be obtained in acidic plating baths.[9]

The crystal structure of the Ni−P alloys as well as their re-crystallization has been determined by X-ray diffraction (XRD), electron diffraction, or transmission electron microscopy (TEM) and differential scanning calorimetry (DSC)[7,8] and, more recently, by magnetothermal studies.[10,11] The overall crystallization process consists of an eutectic transformation with Ni and Ni_3P as final products at high temperature, preceded by a primary crystallization at low temperatures of Ni in the hypoeutectic alloys (phosphorus 15−19 at. %) and of Ni, Ni_3P, and Ni_2P_5 phases in the hypereutectic alloys (phosphorus > 20 at. %). Primary crystallization at low temperature is absent in the alloys with eutectic com-

* To whom correspondence should be addressed.
[†] Università degli Studi di Cagliari.
[‡] Warsaw University of Technology.
[§] Istituto di Struttura della Materia CNR.
[||] Università "La Sapienza" di Roma 1.

(1) Grimsley, S. *Trans. Inst. Met. Finish.* **2002**, *B4*, 80.
(2) Diegle, R. B.; Sorensen, N. R.; Nelson, G. C. *J. Electrochem. Soc.* **1986**, *133*, 1769.
(3) Królikowski, A. Passive Characteristics of Amorphous Ni−P alloys. In *Modifications of Passive Films*; Marcus, P., Baroux, B., Keddam, M., Eds.; The Institute of Materials: London, 1994; p 119.
(4) Li, H.; Li, H.; Dai, W. L.; Wang, W.; Fang, Z.; Deng, J. F. *Appl. Surf. Sci.* **1999**, *152*, 25.
(5) Suganuma, Y.; Tanaka, H.; Yanagisawa, M.; Goto, F.; Hatano, S. *IEEE Trans. Magn.* **1982**, *18*, 1215.
(6) Haidu, J. *Trans. Inst. Met. Finish.* **1997**, *75* (1), B7.
(7) Hur, K. H.; Jeong, J. H.; Lee, D. N. *J. Mater. Sci.* **1990**, *25*, 2573.
(8) Révész, A.; Lendvai, J.; Loranth, J.; Padar, J.; Bakonyi, I. *J. Electrochem. Soc.* **2001**, *148* C715.
(9) Krasteva, N.; Armyanov, S.; Georgieva, J.; Avramova, N.; Fotti V. *J. Electron. Mater.* **1995**, *24*, 941.
(10) Tachev, D.; Iorgov, D.; Armyanov, S. *J. Non-Cryst. Solids* **2000**, *270*, 66.
(11) Armyanov, S.; Tachev, D. *J. Non-Cryst. Solids* **2003**, *328*, 250.

10.1021/cm030606x CCC: $27.50
Published on Web 10/01/2004

position (19−20 at. % P). This crystallization process has received new interest as a possibility to obtain nanocrystalline Ni−P alloys that can be produced by controlling the heating procedure, time, and temperature of the transformation.[8,12]

Whereas in structural studies of crystalline or re-crystallized Ni−P alloys clear diffraction peaks of nickel and Ni_3P phases are found, these well-defined peaks disappear with increasing phosphorus content and only a broad, unresolved peak between 40 °C and 50 °C appears.[7,8] This is usually interpreted as absence of long-range translational order characteristic of crystalline alloys.[13] However, this broad X-ray diffraction pattern of "X-ray amorphous alloys" might be an uncertain basis for deciding whether a structure is amorphous or nanocrystalline because it is well-known that diffraction peaks become progressively wider and less intense as the average grain size decreases.[14,15] So the "true" structure of the "amorphous" Ni−P alloys is still under discussion; the more recent literature considers these alloys nanocrystalline. More powerful techniques such as neutron diffraction methods, particularly isotopic substitution neutron diffraction, have been used to obtain more detailed information on the alloy structure.[16] From these measurements total and partial pair correlation functions in metallic glasses were determined.[16] For the amorphous Ni−P alloys with 20 at. % phosphorus a Ni−Ni distance of 2.56 Å was calculated in agreement with earlier results from XRD,[7] corresponding closely to the atomic diameter of nickel (2.48 Å) whereas the Ni−P distance of 2.26 Å yields an apparent diameter of the P metalloid atom of ca. 2 Å, much smaller than the atomic diameter of phosphorus (2.56 Å). In addition, from the P−P distance of 3.73 and 4.30 Å, respectively, the metalloid atoms do not appear as nearest neighbors but at larger distances in a coordination shell around 4 Å, which is split into two subshells.[16] From these features it was concluded that the structure of the amorphous Ni−P alloy is not "random" but governed by a chemical ordering effect due to chemical interaction between the Ni atoms and the metalloid P.[17]

This chemical interaction, precisely the chemical state of nickel and phosphorus and the electronic structure of amorphous Ni−P alloys, are studied best by X-ray photoelectron spectroscopy (XPS). The binding energies of core-level electrons in general provide chemical state information about near-surface atoms or ions. From a previous work of some of the authors,[18] the oxidation state of phosphorus in the Ni−P alloys was found to be slightly negative with respect to elemental phosphorus, indicating the formation of partially covalent bonds with nickel. For nickel the determination of the chemical state based on XPS binding energies is not always possible: the binding energy range of $Ni2p_{3/2}$ electrons for Ni metal and conducting nickel compounds (NiS, NiAs, etc.) are similar within ca. 0.2 eV [ref 19 and literature cited therein]. Apparently, the ligand (here phosphorus) has little effect on the Ni2p main line binding energies. The only systematic difference observed in changing from metallic nickel to NiS or NiAs[19] was an increase of the binding energy separation between the satellite and the main peak of the Ni2p spectra. As a consequence, it is the binding energy of the satellite peak that is influenced by the presence and nature of the ligand and should be influenced also by the coordination shell and nearest number of phosphorus atoms; thus, XPS should reveal differences—if present—in the electronic structure of Ni−P alloys between amorphous and re-crystallized state.

In this work, the structural changes (phase transitions) during the crystallization of the nearly eutectic electrodeposited Ni−P alloy with 22 at. % of phosphorus (Ni22P) have been studied by energy-dispersive X-ray diffraction (EDXD), collecting the diffraction pattern statically with a simple experimental setup that requires no movement of the sample. Changes in the chemical state and electronic structure have been investigated by X-ray photoelectron spectroscopy (XPS). The combination of these complementary techniques and of the results—to our knowledge—is new and can provide new insights into the crystallization process of Ni−P alloys.

2. Experimental Section

2.1. Synthesis of Ni−P Alloys. Ni22P alloys were obtained by electro-deposition on copper foil. Prior to deposition, the substrate was degreased in an alkaline solution and etched in H_2SO_4 solution. The substrate was masked with lacquer to have an effective plating area of 42 × 80 mm^2. The electrodeposition of Ni−P was carried out under galvanostatic control. The plating solution contained 0.64 M nickel sulfate ($NiSO_4$), 0.11 M sodium hypophosphite (NaH_2PO_2), 0.5 M phosphoric acid (H_3PO_4), 0.33 M boric acid (H_3BO_3), and 0.33 M sodium chloride (NaCl), and the solution pH was 1.8, temperature 70 ± 1 °C, current density 2.7 A/dm^2, and plating time 150 min. All reagents were of analytical grade.

An anode of pure Ni was placed in a filter bag. Special care was taken to ensure the deposit uniformity. Ni−P electrodeposits usually show some lowering in P content with thickness going from the substrate to the top due to the rise in pH and bath depletion in hypophosphite. To avoid this, a high ratio bath volume/deposited surface area was here employed, together with a periodical correction of pH, and vigorous stirring. Some approaches to compositional depth profiling (X-ray microprobe with different penetration depths, analysis of deposits obtained in sequence) were performed and uniform distribution of P, within the experimental errors, was found. The substrate was mounted on an oscillatory holder to stir the solution at the cathode and prevent hydrogen bubbles adhering to the growing deposit. The plating time was adjusted to obtain 30−40 μm thick coatings, which were found to be poreless. Details of the electro-deposition procedure are provided in ref 20.

2.2. Chemical Analysis, ADXD, Thickness Measurements. The alloy composition was determined by wet chemical analysis. Deposits were dissolved in boiling nitric acid. Atomic absorption spectroscopy was used for determining nickel whereas the amount of phosphorus was quantitatively deter-

(12) Lu, K. *Mater. Sci. Eng. R* **1996**, *16*, 161.
(13) Elliott, S. R. *Physics of Amorphous Materials*, 2nd ed.; Longman Scientific and Technical: London, 1990.
(14) Bredael, E.; Blanpain, B.; Celis, J. P.; Ross, J. R. *J. Electrochem. Soc* **1994**, *141*, 294.
(15) Itoh, K.; Wang, F.; Watanabe, T. *J. Jpn. Inst. Met.* **2001**, *65*, 495.
(16) Lamparter, P. *Phys. Scr.* **1995**, *T57*, 45.
(17) Lamparter, P. *Phys. Scr.* **1995**, *T57*, 72.
(18) Rossi, A.; Atzei, D.; Elsener, B.; Krolikowski, A. Electrochemical and XPS Surface Analytical Characterization of Amorphous Electrodeposited Ni−P alloys. Proc. Int. Conf. EUROCORR 2001, 30.9. − 4.10.2001 Gargnano (It) on CD.
(19) Nesbitt, H. W.; Legrand, D.; Bancroft, G. M. *Phys. Chem. Miner.* **2000**, *27*, 357.
(20) Krolikowski, A. *Mater. Sci. Forum* **1995**, *185−188*, 799.

mined by the phosphomolybdate blue method.[21,22] The NiP alloy under study contained 22 at. % P (ca. 14 wt %).

The structure of this alloy was tested by conventional ADXD (angular-dispersive X-ray diffraction, see section 2.3) measurements. By previous investigations, samples of this kind with less than 12 at. % P were found to be crystalline; samples containing more than 18 at. % P showed X-ray amorphous structures. For the transitional range, 12−16% P, either crystalline or amorphous structures were revealed.[23] According to this statement, the sample under testing exhibited an amorphous structure, as will be shown in the section dedicated to diffractometry.

The thickness of the NiP layer was estimated by measuring the weight gain during deposition. The applicability of this approach was proven by observation of a polished cross section of coatings under a metallographic microscope. The sample was about 40 μm thick.

2.3. The EDXD Technique and Its Application to Phase Transitions. An ordinary ADXD diffractogram represents the intensity of a monochromatic radiation diffracted by the sample as a function of the scattering angle 2ϑ. In this case, also the energy E (or, equivalently, the wavelength) of the X-ray radiation utilized has to be specified. Changing the radiation energy, each diffraction peak is shifted to a different angular value (higher if the energy is decreased and vice versa). Instead, if the diffracted intensity is expressed in terms of the scattering parameter q, a universal diffractogram independent of the radiation energy is obtained. The scattering parameter q represents the momentum transferred from the radiation to the sample and can be expressed as follows

$$q = \frac{2}{hc} E \sin \vartheta$$

where c is the speed of light, h is Planck's constant, E is the energy of radiation, and ϑ is the scattering angle. According to this expression, a q scan can be performed in two ways. The first is the aforementioned conventional ADXD method, which consists of using a monochromatic radiation (E fixed) and carrying out an angular scan. Alternatively, a continuous spectrum radiation, containing photons of any energy up to a maximum value, can be used. In the latter case, the angle ϑ is kept unchanged during the acquisition and the technique is called energy-dispersive X-ray diffraction (EDXD). In the EDXD measurements, a solid-state detector capable of distinguishing the chromatic components of the diffracted spectrum executes the energy scan.

A detailed treatment of the advantages of the latter method can be found in refs 24−28. Summarizing briefly, in EDXD no sample or detector motion is required; thus, the analyzed area and the scattering volume of the sample is constant. Complex experimental devices such as the high-temperature chamber used in this work can be easily utilized due to the simple geometrical arrangement. In addition, the integrated intensity of the white radiation utilized as the primary beam is one order of magnitude higher than that of the fluorescence line used in ADXD in the same working conditions. As a consequence, a proportional decrease of the acquisition times at a parity of statistical accuracy is obtained. Furthermore, the higher energy of radiation increases the penetration of the X-rays into the material under testing. This allows measurements on metallic samples in the transmission geometry, which is more reliable since the optical paths of X-rays are independent of both the photon energy and the scattering depth. For this reason, the EDXD technique was used to follow the time evolution of the system upon heating, while the ADXD technique (due to its higher resolution) was used to investigate the system in static conditions.

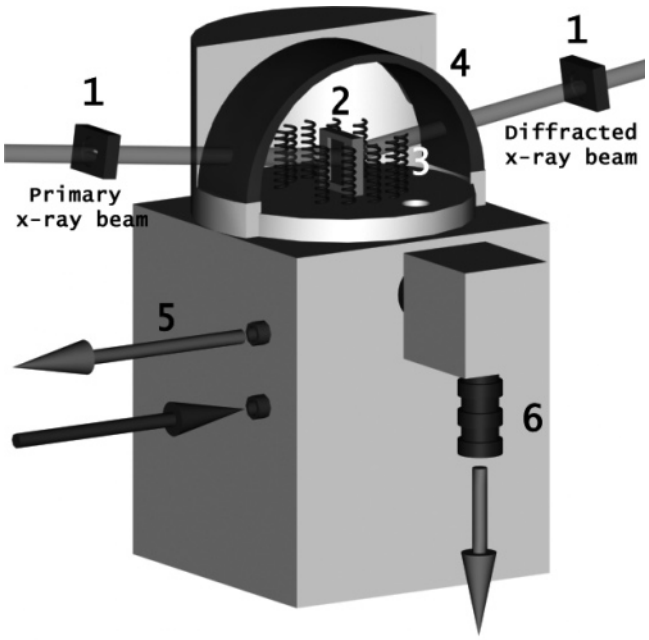

Figure 1. Picture of the custom high-temperature chamber. (1) Collimation slits, (2) sample holder, (3) heating system (crown of spiral-shaped electrical resistances), (4) cylindrical beryllium window, (5) refrigerating system, (6) evacuation pipe.

The Chamber. The high-temperature chamber is constituted by a sample holder surrounded by a crown of electrical resistances (see Figure 1) connected to a power supply. A feedback thermocouple controls the current flowing through the heating resistance**,** such that the temperature is stable within 1 °C. The cover of the sample holder is a stainless steel block with a cylindrical beryllium window to allow the passage of the X-ray radiation. After the cover is closed, a turbomolecular pump provides a working pressure of 10^{-4} Pa in the chamber. A hydraulic refrigerating system maintains the temperature of the external part of the chamber close to room temperature.

The Diffractometer. A noncommercial EDXD diffractometer was used in this work.[29] It is provided with a usual tungsten anode X-ray tube. In the present measurements, the angle ϑ was set at 11°. The beam produced by the X-ray tube is not monochromatized (white) but just collimated by two W slits to reduce its angular divergence. The source is an Italstructure, fine-focus (0.4 mm × 8 mm) tube, whose maximum power is 2 kW. The working conditions were 55 kV and 25 mA. The beam enters the high-temperature chamber through the beryllium window and impinges the NiP sample (ca. 40 μm thick) in the transmission configuration. The scattered beam is collimated in the same way as the incident one and reaches the energy-dispersive detector. The energy-dispersive detector, manufactured by EG&G-Ortec company (GLP series), is provided with a planar high-purity Ge crystal as its sensitive

(21) Marczenko, Z.; Balcerzak, M. *Separation, Preconcentration and Spectrophotometry in Inorganic Analysis*; Elsevier: Amsterdam, 2000; p 326.

(22) Bielinski, J.; Bielinska, A. *Inzynieria Powierzchni* **1998**, *3* (2), 3.

(23) Krolikowski, A.; Butkiewicz, P. *Electrochim. Acta* **1993**, *38* (12), 1979.

(24) Caminiti, R.; Sadun, C.; Bionducci, M.; Buffa, F.; Ennas, G.; Licheri, G.; Musinu, A.; Navarra, G. *Gazzetta Chim.* **1997**, *127*, 59.

(25) Olsen, J. S.; Gerward, L.; Jiang, J. Z. *J. Phys. Chem. Solids* **1999**, *60*, 229.

(26) Caminiti, R.; Isopo, A.; Orru, M. A.; Rossi Albertini, V. *Chem. Mater.* **2000**, *12*, 369.

(27) Jiang, J. Z.; Olsen, J. S.; Gerward, L.; Abdali, S.; Eckert, J.; Schlorke-de Boer, N.; Schultz, L.; Shi, P. X. *J. Appl. Phys.* **2000**, *87*, 2664.

(28) Rossi Albertini, V.; Isopo, A.; Caminiti, R.; Tentolini, U. *Appl. Phys. Lett.* **2002**, *80*, 775.

(29) Caminiti, R.; Sadun, C.; Rossi, V.; Cilloco, F.; Felici, R. *XXV Congress on Physical Chemistry*, Cagliari, Italy: 1991. Caminiti, R.; Sadun, C.; Rossi, V. Apparecchiatura per la misura della diffrazione e della riflettometria X da campioni solidi e liquidi. Patent No. RM/93 01261484 June 23, 1993.

element and is suitable to detect X-ray photons below 150 keV. Thus, this detector is capable of distinguishing the energy of the photons contained in the scattered beam, producing a current pulse whose intensity is proportional to the energy of the absorbed photon. In this way, the number of pulses equals the number of photons and the time integral of each pulse accounts for the photon energy. The detector is connected to a Multi Channel Analyzer (EG&G Ortec 92-X Spectrum Master), which digitally reconstructs the spectrum of the scattered radiation. The final result is a diffractogram in the form of a histogram: its x-axis is divided into small intervals of the same amplitude (channels) proportional to the energy, while the integer value contained in each channel represents the number of photons detected at that energy.

Measurement Procedure. The sample was put in the high-temperature chamber, which was evacuated after closing, and heated in a time negligible in comparison to the duration of the measurements. The sample was then submitted to a sequence of irradiations, lasting Δt=500 s each, and the resulting diffractograms were recorded providing, in this way, a description of the structural evolution of the system under testing.

In this way, it was possible to calculate the coordinate $x(t)$, which represents the stage of the sample transformation at the instant t, just doing a comparison among the raw spectra, with no need of processing or correcting them. $x(t)$ can be obtained[30] as the average over q of the ratio $[I(q,t) - I(q,t_1)]/[I(q,t_2) - I(q,t_1)]$, where $I(q,t)$ is the intensity scattered in correspondence of a q value in the generic instant t, while t_1 and t_2 are the beginning and the end of the transition, respectively. Indeed, the intensity of each white X-ray beam scattered by a sample can be expressed as the sum of different quantities, namely, coherent (or Thomson's) and incoherent (or Compton's) single scattering contributions and multiple scattering contribution. These quantities are all weighted by coefficients characteristic of the scattering process (intensity, polarization, and X-ray absorption of the incident beam). If the density of the alloy does not change much upon (re)-crystallization of the sample (as in the present case), the coefficients of the scattering process and the incoherent contribution are almost constant. Neglecting the multiple scattering, which is small when the sample is thin like ours, the only quantity that changes during the phase transition is the coherent single scattering, that is to say, the diffracted intensity.

This simplifies the experimental procedure very much, prevents artifacts, and makes the EDXD method for phase transitions easy to apply. The parameter $x(t)$ obtained is the equivalent of the reaction coordinate for chemical transformations. It is defined as the portion of the sample that has turned to the final phase at the time t, so that its value is zero at the beginning and unit at the end of the process. Through x, the transformation rate can be parametrized by means of the time derivative of x, i.e., in terms of the adimensional parameter $[dx(t)/dt]\cdot\Delta t$. Finally, Liquori's phenomenological model for phase transitions was used for checking on the correctness of x vs t curves profile.[37] Indeed, several structural transitions can be activated thermally in the (initially) amorphous samples. Therefore, to observe and analyze the various processes separately, it is necessary to be sure that a process is concluded before increasing the temperature to activate the successive process; otherwise, a mix of the two would be detected.

2.4. X-ray Photoelectron Spectroscopy (XPS). XPS analyses were performed with an ESCALAB spectrometer (Vacuum Generator Ltd., U.K.). The vacuum system consists of a turbo-molecular pump, fitted with a liquid nitrogen trap and a titanium sublimation pump. The residual pressure in the spectrometer during the data acquisition was always lower than 5×10^{-6} Pa. The specimens were mounted on a metallic sample holder and the surface was covered with a gold mask to allow the analysis of ca. 1 cm^2. The X-ray source was a non-monochromatic Al Kα (1486.6 eV) twin anode run at 20 mA and 15 kV. This source allows measuring the P-Auger lines with higher kinetic energies using the Bremsstrahlung. The X-ray angle of incidence with respect to the surface normal is 30°; the photoemission angle with respect to the surface normal is zero. The transmission function was found to be proportional to $KE^{-0.5}$.[31] All the spectra were obtained in the digital mode (VG ECLIPSE software on IBM). A constant energy of 20 eV was set across the hemispheres of the electron analyzer operated in the fixed analyzer transmission (FAT) mode, giving a full-width at half-maximum (fwhm) value of 1.1 eV for the Ag $3d_{5/2}$ transition; the PKLL lines and the survey spectra were registered with a pass energy of 50 eV. The instrument was calibrated using the inert-gas-ion-sputter-cleaned reference materials SCAA90 of Cu, Ag, and Au.[32] The binding energy results here presented are the mean value over three independent measurements and the standard deviation has been found to be ±0.1 eV for all the peak positions.

The oxide-free surfaces of NiP alloys were obtained using an AG21 ion gun fitted in the analysis chamber of the spectrometer. Ion etching was performed with Ar^+ at 5 keV, 30 μA for 3 min; the residual pressure was 10^{-4} Pa during etching. Under these conditions no preferential sputtering of the NiP alloy was observed and only the removal of the external layers (contamination and oxidized layer) was accomplished.

3. Results

3.1. EDXD Measurements. A series of preliminary tests was performed to establish the link between the temperatures of transition and the corresponding time of transition.[33] Then the measurements were carried out in the way discussed above. The first and the last diffractograms obtained on the initially amorphous alloy with P content of 22% at the lowest transition temperature of 250 °C is shown in Figure 2a. At the beginning essentially two broad peaks at 3.08 and 5.21 Å^{-1}, respectively, together with a shoulder around 7.50 Å^{-1} could be observed. During the 290 X-ray irradiations (up to 39 h) at 250 °C, the main peak splits in three peaks at 4.94, 5.25, and 5.59 Å^{-1}. The broad peak at 3.08 Å^{-1} develops into a sharp intense peak at 3.22 Å^{-1} and a small one at 2.97 Å^{-1}, other minor peaks appearing at 3.67, 3.90, 4.14, 4.60, and 6.52 Å^{-1}, respectively. This peak splitting indicates that the broad peaks arising from the nanocrystalline material are actually several overlapped peaks that become apparent following crystal growth.

After 39 h from the beginning of the heating the diffractogram did not change anymore and the sample had reached its stable configuration at 250 °C.

The temperature was increased until 340 °C, inducing further structural change as shown by the diffractograms in Figure 2b. In this case, the temperature was held at 340 °C for 24 h, but preliminary measurements had been carried out for a longer time (about 1 week) to be sure that no further transformation occurred at that temperature in 24 h. The main peaks at 4.94 and 5.59 Å^{-1} remained constant in position, while the peak at 5.25 Å^{-1} disappeared. Furthermore, the diffraction

(30) Caminiti, R.; Rossi, V. *Int. Rev. Phys. Chem.* **1999**, *18*, 263.
(31) Seah, M. P. *Surf. Interface Anal.* **1993**, *20*, 243.
(32) *Surface Chemical Analysis − X-ray Photoelectron Spectrometers − Calibration of energy scales*; ISO 15472:2001; International Organization for Standardization: Geneva, Switzerland, 2001.
(33) Isopo, A.; Rossi Albertini, V.; Tentolini, U.; Caminiti, R. *J. Appl. Phys.* **2003**, *94*, 1521.
(34) Bonino, J. P.; Bruet-Hotellaz, S.; Bories, C.; Pouderoux, P.; Rousset, A. *J. Appl. Electrochem.* **1997**, *27*, 1193.
(35) Schaerli, M.; Brunner, J. *Z. Phys. B* **1981**, *42*, 285.
(36) Avrami, V. *J. Chem. Phys*. **1939**, *7*, 1103.
(37) Liquori, A. M.; Tripiciano, A. *Proceedings of Volterra Symposium on Mathematical Models in Biology*; Barigozzi, C., Ed.; Springer-Verlag: New York: 1980; p 400.

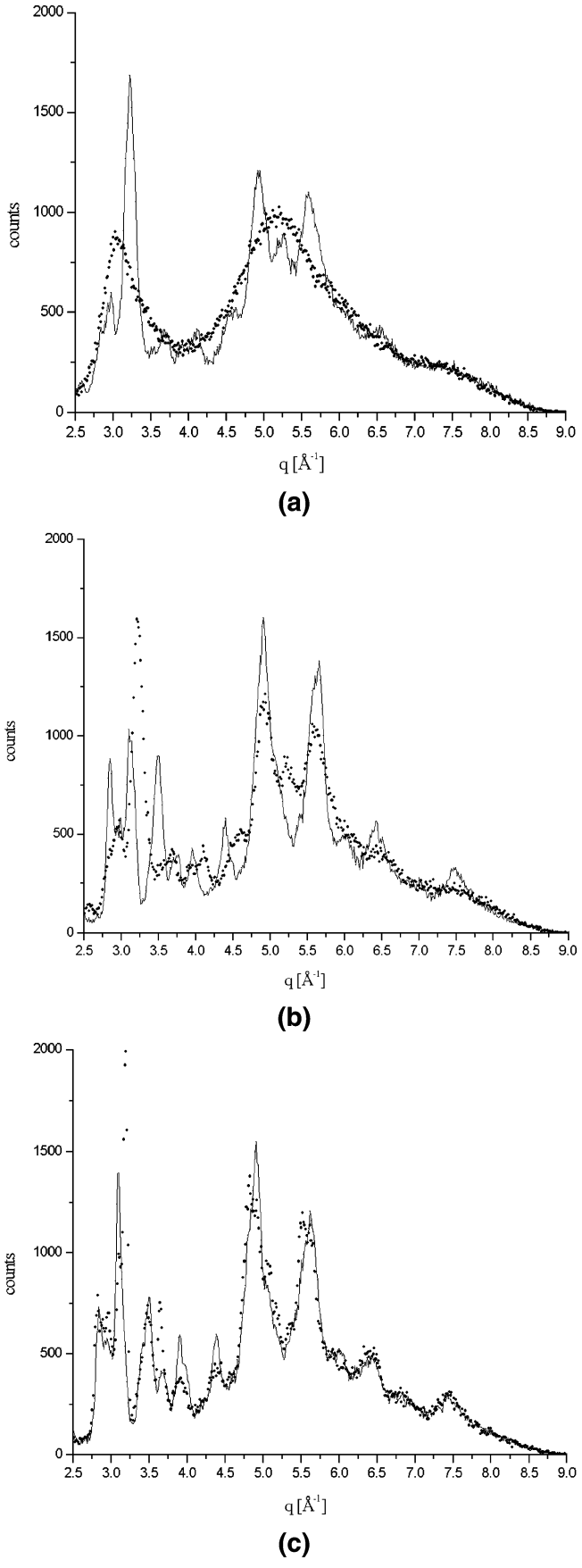

Figure 2. Diffraction patterns of the Ni22P alloy recorded with the EDXD technique. (a) Comparison of the first and last diffraction pattern at 250 °C. (b) Comparison of the first and last diffraction pattern at 340 °C. (c) Comparison of the first and last diffraction pattern at 645 °C.

pattern became richer and more structured due to the appearance of numerous new reflections (see Figure 2b).

Increasing again the temperature up to 520 °C, the spectra did not change anymore, showing that the crystallization taking place at 340 °C was completed, in agreement with DTA analyses.[34]

Finally, the temperature was increased once more until 645 °C. This is the highest temperature of re-crystallization observed below the melting point. However, as can be seen in Figure 2c, the diffractograms showed only slight modifications, the peaks becoming a little more intense and sharp but substantially unchanged. The entire real-time sequence of the diffraction pattern is shown in Figure 3a.

3.2. XPS Results. XPS spectra of the Ni22P alloy in the amorphous state and after complete re-crystallization at 645 °C (as described above) were recorded after argon ion sputtering for 3 min in order to remove only the outermost layers. The quantitative analysis confirmed the composition of the bulk alloy: this indicates that no preferential sputtering occurred. For comparison the spectra of Ni_3P powder were recorded, too. As an example the survey spectrum of the re-crystallized alloy after argon ion sputtering for 3 min is shown (Figure 4). Only signals from nickel and phosphorus are revealed; carbon contamination and oxygen are absent.

In the following, the high-resolution XP spectra of the Ni2p, P2p, P2s, and the X-ray excited PKLL Auger signal of the electrodeposited alloy Ni22P in the amorphous and re-crystallized state together with the spectra of Ni_3P powder are shown. The corresponding binding energies are summarized in Table 1 for $Ni2p_{3/2}$, $Ni2p_{1/2}$, P2p, and P2s together with the kinetic energy of the PKLL signal.

Nickel Ni2p Region. The high-resolution XPS spectra of the Ni2p region (Figure 5) show a clear distinction between metallic nickel, the Ni22P alloy in the amorphous and re-crystallized state, and Ni_3P powder, respectively. The binding energy of the $Ni2p_{3/2}$ and $Ni2p_{1/2}$ main peaks remains almost constant (Table 1), but the position of the satellite (distance from the $Ni2p_{3/2}$ line) increases from metallic nickel, the Ni22P alloy in the re-crystallized state to the Ni_3P powder (Figure 5, Table 1). In XPS analysis a change in chemical environment or oxidation state of an atom usually is accompanied by a change in binding energy of the atom (concept of chemical shift[45]); e.g., a change from metallic nickel to nickel oxide or nickel hydroxide results in an increase of the binding energy of the Ni2p signal (Table 1). A constant binding energy of the Ni2p signal as found

(38) Kumar, P. S.; Nair, P. K. *J. Mater. Process. Technol.* **1996**, *56*, 510.
(39) Lashmore, D. S.; Bennett, L. H.; Schone, H. E.; Gustafson, P. S.; Watson, R. E. *Phys. Rev. Lett.* **1982**, *48*, 1760.
(40) Hüfner, S. *Photoelectron Spectroscopy*, 2nd ed.; Solid State Sciences; Springer: Heidelberg: 1996; p 74 and literature cited herein.
(41) Elsener, B.; Krolikowski, A.; Atzei, D.; Rossi, A. An XPS and X-AES investigation on the electronic structure of nanocrystalline Ni−P electrodeposited alloys. To be published.
(42) Suzuki, K.; Itoh, F.; Fukanaga, T.; Honda, T. *Rapidly Quenched Metals III*; Contor, B., Ed.; The Metals Society: London, 1978; Vol. 2, p 410.
(43) Ratzker, M.; Lashmore, D. S.; Pratt, K. W. *Plat. Surf. Finish.* **1986**, *73* (9) 74.
(44) Chen, N.; Feng, P.; Sun, J. The electronic structure of Ni−P and Pd−Ni−P glasses; In *Rapidly Quenched Metals*; Steeb, S., Warlimont, H., Eds.; Elsevier Science Publishers: New York, 1985; p 999.
(45) Egelhoff, W. F., Jr. *Surf. Sci. Rep.* **1987**, *6*, 253.

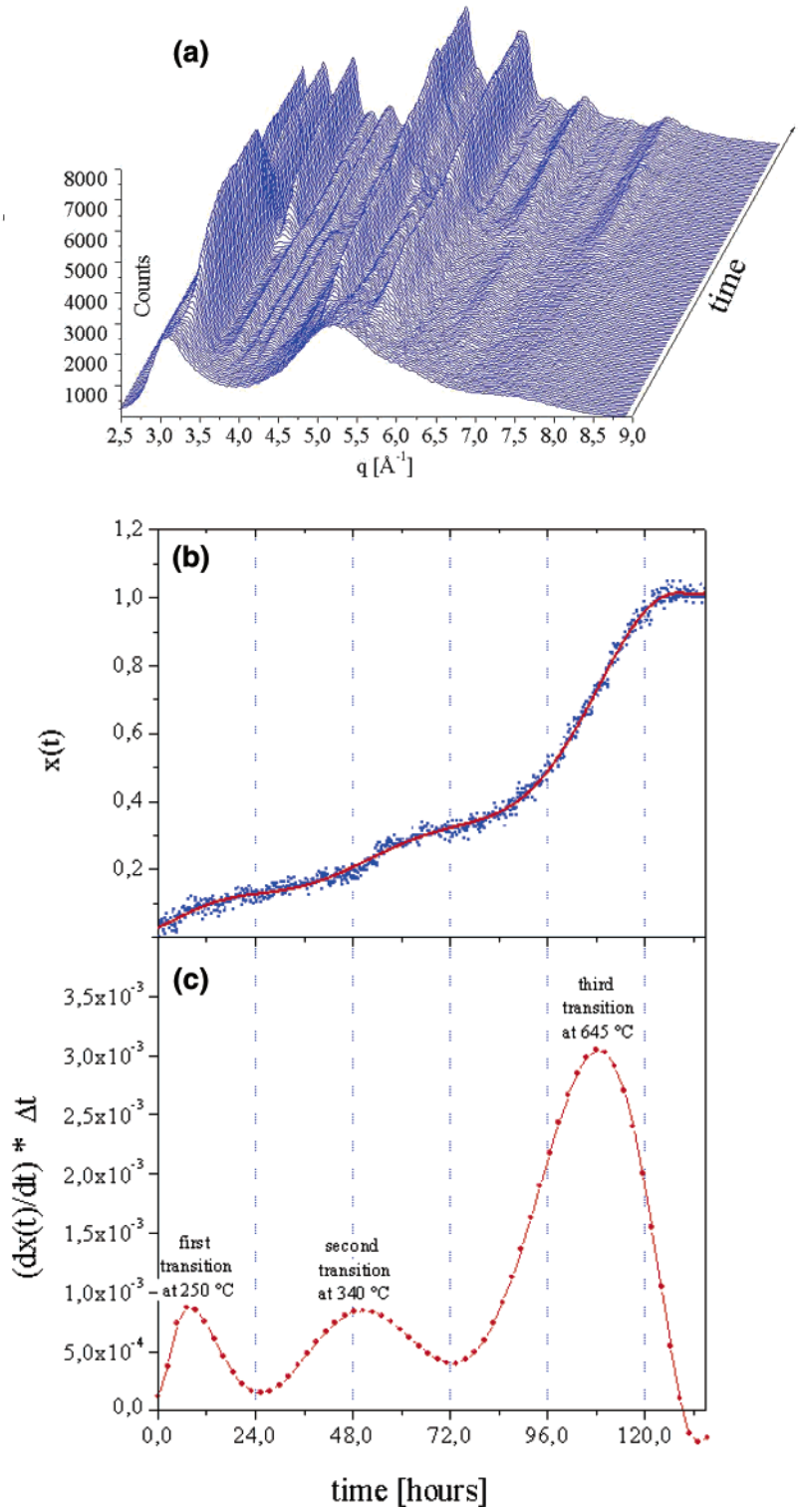

Figure 3. (a) Sequence of the diffraction patterns collected during crystallization. (b) Plot of the transition coordinate $x(t)$. (c) Time derivative $dx(t)/dt\ \Delta t$. The peaks represent the highest transition rates of the system, while the minima indicate the presence of intermediate steady states.

for the NiP alloys (Table 1, Figure 5) however cannot be interpreted in a straightforward manner as there has been no change in the chemical environment or oxidation state of the nickel atom as has been shown for conducting nickel compounds such as Ni, NiS, and NiAs.[19] In the case of conducting nickel compounds such as Ni−P alloys, the detailed analysis of the main peak/satellite structure becomes particularly important. Indeed, in this work the binding energy difference main peak/satellite increases from metallic nickel (5.7 eV) to sputtered Ni_3P powder (7.2 eV), indicating a change in the electronic structure.

Phosphorus P2p and P2s Region. The high-resolution signals of the phosphorus P2p region are shown in Figure 6. The sputter-cleaned Ni22P alloy in the amorphous as well as in the re-crystallized state show a single peak at a binding energy of 129.4 eV. The doublet $P2p_{3/2}/P2p_{1/2}$ was fitted with an energy difference of 0.9

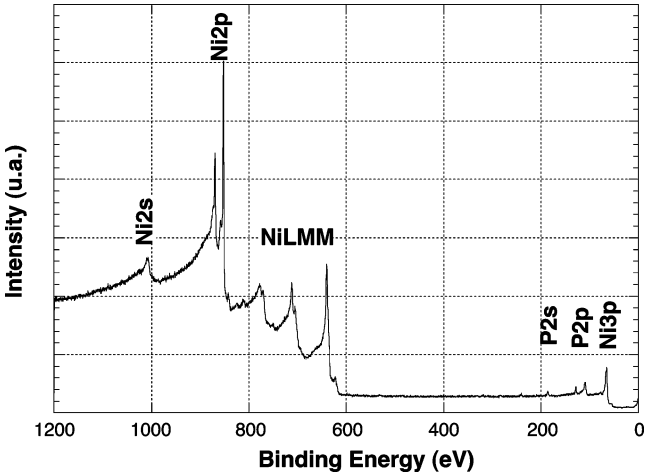

Figure 4. XPS survey spectrum of sputter-cleaned Ni22P alloy after re-crystallization at 645 °C. Al Kα 300 W, pass energy 50 eV.

Table 1. Binding Energies of the Ni2P, P2P, and P2s and Kinetic Energy of the PKLL Signals (Amorphous and Re-crystallized Ni22P Alloy, Reference Compounds, Sputter Cleaned)[a]

sample	$Ni2p_{3/2}$ (eV)	$Ni2p_{1/2}$ (eV)	Ni sat (eV)	Δsat (eV)	P2p (eV)	P2s (eV)	PKLL (eV)	sat (eV)
Ni22P amorph	852.8	870.1	859.2	6.4	129.4	187.2	1858.2	1850.8
Ni22P recryst	852.8	870.0	858.8	6.0	129.4	–	1858.2	1850.8
Ni_3P powder sp	852.9	870.1	860.2	7.2	129.5	–	1858.0	1850.9
Ni metal	852.8	870.1	858.5	5.7	–	–	–	–
NiO	854.8	–	856.1 861.5	1.3 6.7				
$Ni(OH)_2$	856.3	–	857.3 862.4	1.0 6.1				

[a] Data for NiO and $Ni(OH)_2$ are included for comparison. The standard deviation is found to be ±0.1 eV for all the peak positions.

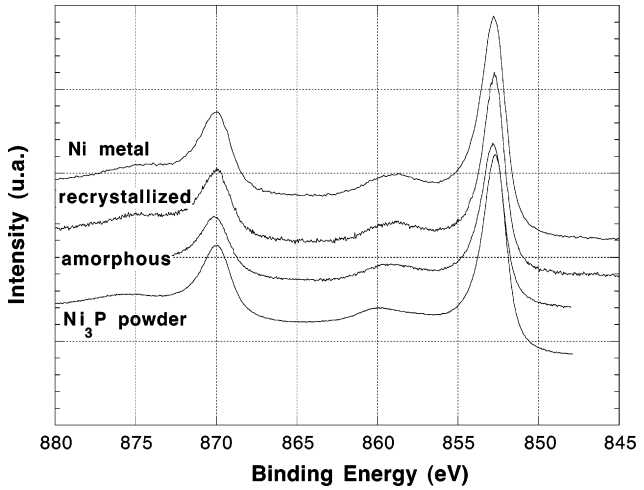

Figure 5. High-resolution XPS spectra of the Ni2p region comparing the Ni22P alloy in the amorphous and re-crystallized state with metallic nickel and Ni_3P powder. Al Kα 300 W.

eV and a ratio of 0.5. The Ni_3P powder shows the same peak; in addition, a second P2p doublet is revealed at 133.7 eV corresponding to the oxidized surface of the powder. The binding energies are summarized in Table 1. The binding energies of the P2s signal (Table 1) confirm the results of the P2p signal.

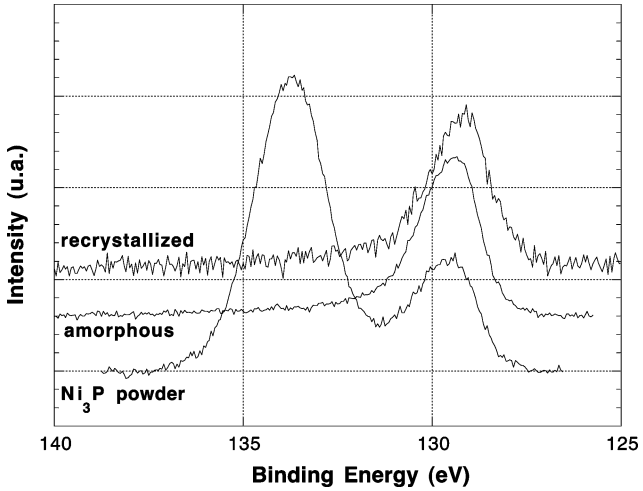

Figure 6. High-resolution XPS spectra of the P2p region comparing the Ni22P alloy in the amorphous and re-crystallized state with Ni_3P powder as received. Al Kα 300 W.

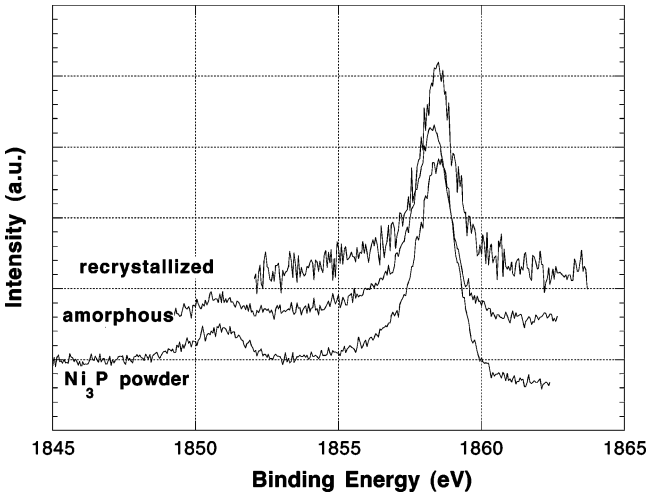

Figure 7. High-resolution spectra of the X-ray excited PKLL Auger signals comparing the Ni22P alloy in the amorphous and re-crystallized state with Ni_3P powder sputtered. Al Kα 300 W.

PKLL Region. The X-ray excited Auger signals (PKLL) of all the samples studied (Figure 7, Table 1) show a main peak at 1858.2 eV. No differences between the re-crystallized or amorphous state of the Ni22P alloy could be detected. An additional small Auger peak was revealed at a constant distance of ca. 7.4 eV from the main peak, independently of the oxidation state of the phosphorus compound. The presence and the difference in energy of this additional Auger peak is in agreement with an earlier work of Schaerli and Brunner.[35]

Summarizing, the nickel and phosphorus more intense photoelectron lines are insensitive to changes in the structure of the Ni22P alloy observed by X-ray diffraction. Ni2p satellite peak shapes however indicate changes in electronic structure. The binding energy of the satellite decreases after re-crystallization of the Ni22P alloy.

4. Discussion

The transition from the amorphous to the crystalline state of binary metallic glasses such as nickel−phos-

phorus in the composition range P > 18 at. %[23] affect both the corrosion resistance[2,3] and the catalytic behavior[4] of the alloys. It is, however, not yet fully established if the changes in properties are due to a change in structure or grain size or due to changes in the electronic structure of the Ni22P alloy or both.

4.1. Change in Morphology and ADXD Structure. As discussed by Braedal et al.,[14] the broadening of the main (111) diffraction peak in electroless deposited NiP alloys can be caused by a decrease in the grain size from 150 to 15 Å. Indeed, on a series of electrodeposited Ni−P alloy films the X-ray diffraction pattern showed a gradual change from sharp to broad peaks with increasing P content.[7,15] HRTEM observation revealed that the crystallographic structure of an electrodeposited 18.5 at. % P alloy was crystalline with a crystal size of about 10 nm. At 21.5 at. % P, a crystal size of 3 nm was found.[15] On the other side, also amorphous Ni−P alloys clearly display short-range order.[16,17] Thus, the NiP alloys with an amount of phosphorus higher than 18 at. % were called X-ray amorphous or topologically long-range disordered.[30] The question if diffraction patterns recorded on electrodeposited as-plated NiP alloys indicate a transition from crystalline to amorphous structure with increasing phosphorus content will not be addressed further here.

In Figure 3a, the energy spectra (i.e., diffractograms) acquired during the transitions have been shown. According to what is discussed in section 2.3, the transition coordinate (Figure 3b) and its derivative (Figure 3c) can be obtained from this sequence. Theoretically, the transition coordinate should be calculated over the q-interval $(0 - \infty)$ but, due to the damping of the diffractograms modulations at high q values, the average in the observed interval represents a very good approximation. Therefore, $x(t)$ is calculated over the accessible q-interval only.

The fact that the changes occur in the same regions of the spectra both at 250 °C (Figure 2a) and 340 °C (Figure 2b) might induce one to think that the first transformation at 250 °C is not complete and further heating just accelerates it. However, according to both Avrami's and Liquori's theory,[36,37] the kinetics of phase transitions have a well-defined progression. In correspondence of each phase transition, they start slowly at the beginning, have a successive sudden onset, and then relax to the final structure (Figure 3b). In terms of the derivative of the reaction coordinate $x(t)$, this means that the transition speed is small at first, then rises, and, finally, decreases again. This agrees with the shape of $dx(t)/dt$ plotted in Figure 3c. Similar curves were found for the transitions at higher temperatures.[33]

Studies on the crystallization of electroless Ni−P deposits with P content between 4.35 and 9.12 wt % (8−16 at. %) indicated a fully annealed state at ca. 400 °C and a change in the micro-hardness in the temperature range between 360 and 400 °C in agreement with this work (at 520 °C no changes to 340 °C were observed). The final stable phase after crystallization at 600 °C was found to be Ni_3P.[38] In a work on the crystallization kinetics and phase transformation of electroless Ni−P alloys with phosphorus content of 12−16 wt % (20−26 at. %), the sequence of phase transformation was found to proceed from amorphous, intermediate metastable phases + Ni_3P, to stable Ni_3P and fcc nickel[39] in agreement with the early work of Hur[7] and this work.

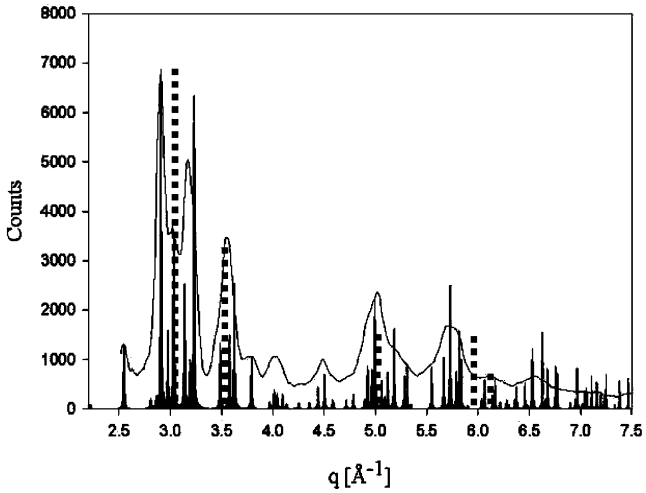

Figure 8. Comparison of the diffraction spectra of the fully re-crystallized electrodeposited Ni22P at. % alloy after normalization to the incident beam spectrum (solid line) with the diffraction spectra of crystalline Ni_3P (black peaks) and with pure Ni (dotted bars).

The q values calculated in this work from the diffraction diagrams (Figure 8) indicate that the crystal structure of the re-crystallized Ni22P alloy after complete re-crystallization at 645 °C closely resembles that of Ni_3P with a minor contribution of crystalline nickel in agreement with ref 7. The Ni_3P phase has been identified as a stable phase formed at re-crystallization at 600 °C.[7,39] The slight shift observed in peak position is due to a little uncertainty on the absolute value of the diffraction angle. Minor differences in peak intensity can be attributed to the fact that the Ni_3P powder taken as reference was composed of relatively big particles whereas the Ni_3P phases supposed to be formed in the re-crystallized alloy have much smaller dimensions and might still be embedded in a fcc nickel matrix.

4.2. Change in Electronic Structure. The high-resolution XPS and XAES spectra of the Ni22P alloy show that the binding energies of the core levels of nickel and phosphorus remain constant (Table 1), differences between the as-plated (amorphous) state and the re-crystallized state can be revealed only in the Ni2p satellite structure (Figure 5, Table 1). Based on the concept of "chemical shift" usually valid in XPS measurements, this would indicate, in a first interpretation, that nickel and phosphorus have the same chemical state irrespective of the crystallographic structure. However, as shown below, the binding energy of nickel in conducting compounds can remain constant despite a change in the chemical environment. The phosphorus atoms (ligands) and their nearest neighbor position (dependent on the structure of the alloy) influence the energetic contributions of the nickel atoms in the alloy.

XPS Signals of Ni Binary Compounds. From the literature it is known that for metallic nickel two distinct final states are possible upon ejection of a core level photoelectron: either $c^{-1}3d^{9}4s^{2}$ or $c^{-1}3d^{10}4s^{1}$.[19,40] These two final states result in two XPS peaks, a main peak and a satellite peak at a binding energy distance of 6−8 eV. The relative intensity of the two peaks is determined by the probability of filling the 4s or the $3d^{9}$

holes. The origin of the two photopeaks is described in ref 40. It has been shown that these main peak/satellite structures hold for all Ni bands (2p, 3s, 3d).[40]

The influence of nonmetallic ligands in conducting nickel compounds such as NiS or NiAs on the difference in binding energy between the two final states (main and the satellite peak) has been discussed.[19] The less intense screening of the core-hole by the fewer "metallic" (nonbonding) 3d electrons of nickel in NiS or NiAs compounds has been proposed as explanation for the higher binding energy of the satellite.[19,40] The same concept can be adopted for the conducting Ni22P alloys studied in this work.

The experimental Ni2p data (Table 1) show that the Ni2p peak binding energies of the Ni22P alloys do not reflect the crystalline structure in which Ni is bonded to phosphorus but the change in crystal structure is accompained by a decrease in the binding energy difference between the $Ni2p_{3/2}$ main peak and the satellite; it decreases from 6.4 eV in the amorphous to 6.0 eV in the re-crystallized Ni22P alloy (Table 1). It is thus shown for the first time that not only the type of ligand (P, S, As)[19] but also the crystal structure changes the electronic structure of the conducting nickel compounds.

4.3. Structural and Chemical Order. From neutron diffraction experiments with isotopic substitution of the nickel atoms, it was concluded[16] that the phosphorus metalloid atoms in amorphous NiP alloys do not appear as direct neighbors (no peak around 2 Å), but they occur as a double peak with a pronounced distance correlation at two different distances around 4 Å. From experiments and Monte Carlo simulation[16,17] the average correlation number of nickel with respect to phosphorus was found to be ca. 9 (with a broad distribution between 8 and 11). This allows us to conclude that the metalloid atoms in the amorphous NiP alloy are *not* distributed randomly in a framework of nickel metal atoms (as assumed in the past) but play a dominant role in the amorphous structure by establishing their own neighbors of about nine metal atoms by chemical interaction with the metal atoms.

On the other hand, the experiments with EDXD technique in this work show clear changes from "amorphous" (broad peaks) to crystalline structure (similar to Ni_3P) after re-crystallization at 645 °C (Figure 8). These changes are not reflected in the high-resolution XPS spectra (Figures 5−7). The only difference revealed is the distance of the final state satellite in the Ni2p spectra (Figure 5, Table 1). A possible explanation of the *insensitivity* of the nickel and phosphorus core lines to structural changes (as revealed by EDXD) in the Ni−P system and simultaneously of the pronounced *sensitivity* of the energy difference of the two final states of the Ni2p core hole after photoionization can be based on the electronic structure of the Ni−P alloys.[42,44] The two XPS photopeaks (main peak and satellite) are the result of two distinct final states. The binding energy difference between the main peak and its satellite is affected by the presence and nature of the ligand (as shown in the literature for P, S, or As,[19,41] the concentration of the ligand,[41] or the structural order (this work, Figure 5). In both, the amorphous and re-crystallized Ni−P alloy, the $3d^9$ band straddles the Fermi level and the $3d^8$ band is ca. 2 eV below the Fermi level and provides equivalent screening in the solids ("metallic", nonbonding electrons). The band of the P2p electrons of Ni−P (molecular orbital of dominantly ligand character, bonding electrons) extends from about 4 to 8 eV below the Fermi level and is not involved in filling the $3d^9$ band. A higher binding energy value of the final state satellite peak corresponds to a deeper potential well after core hole formation,[19,40] hence to a lowered screening of the valence band region due to a higher number of Ni3d bonding electrons (higher density of state at the Fermi level). XPS valence band spectra showed a lower density of state near the Fermi level when adding phosphorus to Ni−Pd alloys,[44] interpreted as covalent bond formation between metal atoms and phosphorus. The reduction of the magnetic susceptibility, Knight shift, and NMR spin relaxation rate (all dependent on the density of states at the Fermi level) of amorphous Pd−Ni−P alloys after phosphorus addition have been explained with this concept.[44] Similar results were reported for a Ni−P alloy with 18.9 at. % phosphorus,[42] where no significant differences between electrodeposited and melt-spun NiP alloys were found.

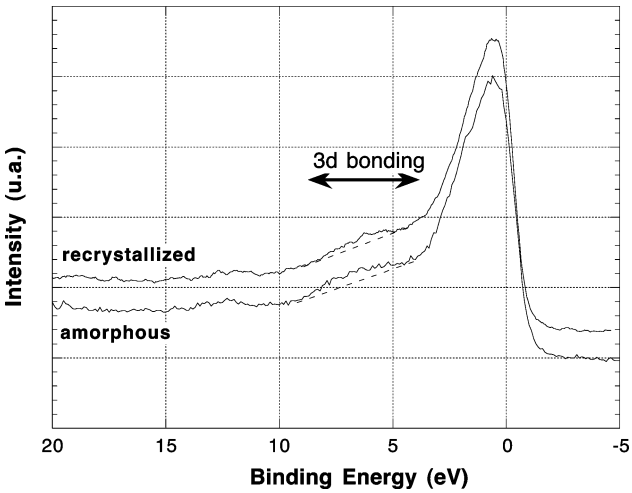

Figure 9. High-resolution spectra of the valence band signals comparing the Ni22P alloy in the amorphous and re-crystallized state. Al Kα 300 W.

A change from the amorphous to the crystalline structure of the electrodeposited Ni22P alloy is accompanied by a decrease in the energy difference between main and satellite peak in the Ni2p spectrum (Table 1). In light of the concept presented previously,[40] the re-crystallized alloy should present a more intense screening, thus a higher number of nonbonding Ni3d electrons or—as a consequence—a lower number of bonding Ni3d electrons located at ca. 4−8 eV below the Fermi level. When the high-resolution valence band spectra (Figure 9) of the Ni22P alloy in the amorphous and re-crystallized state is examined in detail, a higher intensity in the range 4−8 eV can be noted for the amorphous Ni22P alloy; thus, the concept of screening might be substantiated.

5. Conclusions

This combined XPS and EDXD study on thermally induced crystallization of electrodeposited nickel−phosphorus alloy has shown what follows:

EDXD is well-suited to follow in detail the thermally induced crystallization. The (re)crystallization kinetics at all three temperatures applied (250, 340, and 645 °C) follows Liquori's law, as expected. Only at or above 340 °C a complete re-crystallization was observed; the crystallographic phases formed are similar to crystalline Ni_3P.

The XPS Ni2p and P2p core lines as well as the X-ray induced Auger line PKLL do not change in shape and binding energy when the alloy undergoes transition from the amorphous to the fully re-crystallized state. This indicates that re-crystallization does not induce changes in the formal net charge on P and Ni atoms in the alloy. Only the decrease in binding energy difference between the two states in the Ni2p spectra ($Ni2p_{3/2}$ main peak and its satellite) indicates a different electronic structure of the alloy when changing from X-ray amorphous to the crystalline state. It is hypothesized that the amorphous state shows a higher number of bonding Ni3d electrons with respect to the crystallized one. This change in the electronic structure could be verified in the high-resolution valence band spectra of the NiP alloys, where a higher intensity can be noted in the range 4−8 eV below the Fermi level.

In conclusion, the re-crystallization of the electrodeposited amorphous alloy results in a rearrangement of the nearest neighbors of the P and Ni atoms or in other words in the transition from a chemical order (amorphous) to a structural order.

Acknowledgment. Financial support from Italian MURST (60% grant to A. Rossi) is gratefully acknowledged.

CM030606X